ChemComm

Interrogating Biomineralization One Amino Acid at a Time: Amplification of Mutational Effects in Protein-Aided Titania Morphogenesis through Reaction-Diffusion Control

Journal:	*ChemComm*
Manuscript ID	CC-COM-03-2021-001521.R1
Article Type:	Communication

COMMUNICATION

Interrogating Biomineralization One Amino Acid at a Time: Amplification of Mutational Effects in Protein-Aided Titania Morphogenesis through Reaction-Diffusion Control

Received 00th January 20xx,
Accepted 00th January 20xx

DOI: 10.1039/x0xx00000x

Karthik Pushpavanam [a], Brittney Hellner [a] and François Baneyx* [a]

To emulate the control that biomineralizing organisms exert over reactant transport, we construct a countercurrent reaction-diffusion chamber in which an agarose hydrogel regulates the fluxes of inorganic precursor and precipitating solid-binding protein. We show that the morphology of the bioprecipitated titania can be changed from monolithic to interconnected particle networks and dispersed nanoparticles either by decreasing reaction time or by increasing agarose weight percentage at constant precursor and protein concentrations. More strikingly, protein variants with one or two substitutions in their metal oxide-binding domain yield unique peripheral morphologies (needles, threads, plates, and peapods) with distinct crystallography and photocatalytic activity. Our results suggest that diffusional control can magnify otherwise subtle mutational effects in biomineralizing proteins and provide a path for the green synthesis of morphologically and functionally diverse inorganic materials.

Titanium dioxide (titania, TiO_2) is a commodity material used in the formulation of sunscreens, paints and ointments, and in the development of sensors and solar cells, all of which are affected by the materials morphology and phase.[1-3] Since Sumerel *et al.* used silicatein filaments from the sponge *Tethya aurantia* to template the precipitation of an amorphous titania containing nanocrystalline anatase inclusions,[4] a variety of peptides and proteins have been tested for their ability to mineralize TiO_2 under ambient conditions of pressure and temperature (Table S1). Most studies have relied on ammonium oxo-lactato-titanate, a water-soluble precursor known as TiBALDH and recently shown to consist of tetrakis(di-lactato-oxo-titanate) species in equilibrium with tris(lactato-titanate) and ~3-nm anatase nanoparticles capped by lactate ligands.[5, 6] To our knowledge, only two types of bioprecipitates have been obtained in these experiments: titania nanoparticles in the 3 to 50 nm size range and large aggregates consisting of interconnected spherical nanoparticles (Table S1).[7]

We have reported elsewhere[8] that a genetic fusion between superfolder green fluorescent protein (sfGFP) and Car9, a cationic silica-binding peptide of sequence DSARGFKKPGKR, also induces titania precipitation when added at micromolar concentrations to acidified solutions of TiBALDH. The material is largely amorphous but contains a small amount of mostly monoclinic nanocrystallites whose phase can be changed to mostly anatase by using sfGFP-Car9 mutants with reduced propensity to self-associate at silica interfaces[9] as the inducer. This observation notwithstanding, the precipitate morphology is uncontrollable and, as in many of the studies of Table S1, consists of an open and irregularly shaped network of interconnected nanospheres extending to hundreds of micrometers.[8] We postulate that such a recurring morphology may result from an absence of control over reaction and diffusion during bulk bio-precipitation.

Reaction-diffusion (RD) systems offer a means to non-linearly couple chemical reactions with diffusive transport and an opportunity to exert a nonstandard level of control over the formation and assembly of nanomaterials.[10, 11] For instance, the zeolitic imidazolate frameworks ZIF-8 and ZIF-67 were synthesized using a RD system in which 2-methyl imidazole reacted with Zn(II) and Co(II), respectively, in an agar gel matrix.[12] Silver nanoparticles with diameters ranging between 200 and 1000-nm were fabricated through WET stamping, a method that uses an agarose hydrogel stamp to supply a constant concentration of silver nitrate precursor to a sodium alginate film containing potassium dichromate.[13] Similarly, Estroff and coworkers demonstrated fine control over the production of calcite crystals through diffusion-limited growth in agarose hydrogels.[14] Yet, such strategies have seldom been explored in biomimetic synthesis schemes that rely on biomolecules, and especially proteins, as the inducer.

To address this gap, we designed and fabricated the 1D reaction diffusion chamber (RDC) depicted in Fig. 1. We wanted to compare the influence of mutations in the Car9 domain of the fusion protein on the morphology of titania precipitated under diffusion-controlled and previously studied bulk mixing conditions.[8] The design was therefore guided by simulations in the COMSOL software environment to calculate protein and

[a] Department of Chemical Engineering, University of Washington, Box 351750, Seattle, WA, United States

†Electronic Supplementary Information (ESI) available: Experimental and characterization details along with supplementary figures. See DOI: 10.1039/x0xx00000x

precursor concentrations in the reaction zone of the agarose hydrogel, and ensure they would be comparable to those used in bulk precipitation experiments. Device dimensions and reactant concentrations were verified using the parameters of Table S2 to produce a RDC where one-dimensional diffusion is the predominant mode of transport (Fig. S1). Under standard operating conditions, an agarose solution prepared in pH 5.0 citrate buffer is poured in the device and the flanking combs are removed after hydrogel solidification to produce wells in which protein and precursor are loaded (Fig. 1A).The appearance of a narrow white line in the center of the hydrogel indicates the formation of a titania precipitate that can be physically excised for further analysis (Fig. 1B, arrow). In our experiments, the sfGFP scaffold to which the Car9 solid-binding peptide and its variants are fused serves three purposes: (1) it facilitates the high-level expression of all fusion proteins in a soluble form;[8, 9] (2) it provides a robust framework with long-term thermodynamic and proteolytic stability at room temperature,[15] and (3) it offers a simple means to track protein diffusion in the hydrogel through its bright fluorescence(Fig.S2).

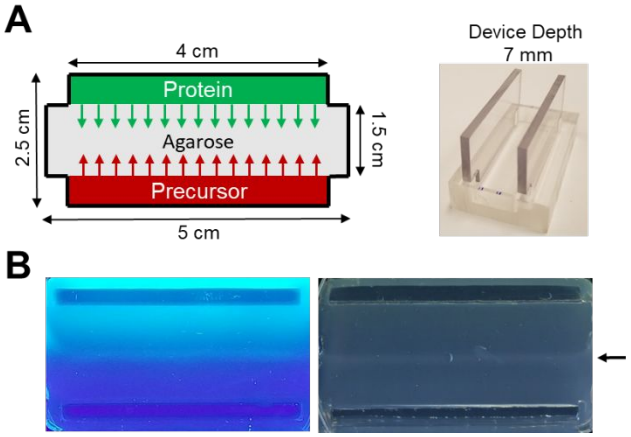

Fig. 1 (A) Schematic (left) and photograph (right) of the RDC. Protein and precursor wells are colored green and red, respectively. (B) Representative in-gel biomineralization experiment. The hydrogel was photographed under UV light (left) or imaged with a flatbed scanner (right) after 24h of reaction. The titania precipitation line is identified by the arrow. The protein was loaded in the top well at 50 µM concentration and allowed to diffuse for 24h before TiBALDH was loaded in the bottom well at 12.5 mM concentration.

We performed preliminary studies to determine optimal conditions for RDC operation, settling on the use of a 0.5% agarose hydrogel, loading the protein 24h prior to loading TiBALDH to produce a well-developed protein gradient under controlled humidity conditions, and terminating the experiment after 24h of reaction. Fig. S3 shows the evolution of the titania precipitated by sfGFP-Car9 under these conditions. (There is no detectable titania precipitation in the absence of protein.) After 6h of reaction, the diffusing TiBALDH has encountered proteins confined in the pores of the agarose hydrogel. Molecules of sfGFP-Car9 have destabilized bound ligands and the cationic solid-binding peptide has helped concentrate the negatively charged precursor at discrete nucleation sites,[16] leading to the growth of isolated TiO_2 particles ~500 nm in diameter through polycondensation reactions (Fig. S3A and S4A). Over the next 6h, and as the transport-limited precursor continues to diffuse in, sfGFP-Car9 continues to induce precipitation, becoming integrated within titania particles that grow to micrometer size and start merging (Fig. S3B and S4B). With further time (t = 18h), particles coalesce with loss of distinct boundaries (Fig. S3C and S4C). Finally, after 24h of reaction, large islands of precipitate that have overcome the mechanical resistance of the H-bonded polysaccharide chains in the agarose network are observed (Fig. S3D and S4D). As we will discuss below, these islands contain unique needle-like structures on their periphery.

The optimization process and a series of control experiments provided additional insights. As expected,[8] sfGFP-Car9 rapidly precipitated bulk titania from acidified solutions of TiBALDH to yield extended (> 100 µm) branched precipitates (Fig. S5). In sharp contrast, use of the RDC chamber with a mechanically strong (1%) agarose hydrogel led to the production of spheroidal particles ranging in size from ~200 nm to 1 µm at the 24h time point (Fig. S6). Substantially similar morphologies were observed when Car9 was fused to the C-terminus of a different protein (mCherry, Fig. S7), when it was appended to the N-terminus of sfGFP (Fig. S8A), or when it was inserted within loop 9 of sfGFP which lies on the opposite side of the β-barrel from the protein's N- and C-termini (Fig. S8B). The fact that neither wild type sfGFP, nor wild type mCherry, could similarly control the formation of nanoparticles in the RDC environment (Fig. S9) implies a critical role of the fused solid-binding peptide in promoting nucleation and in stabilizing nanoparticles by binding to their surfaces. Such capping is however inefficient: as TiBALDH continues to diffuse, titania growth proceeds unfettered, eventually overcoming the mechanical resistance of the polysaccharide network to yield a continuous precipitate after 48h of reaction (Fig. S10).

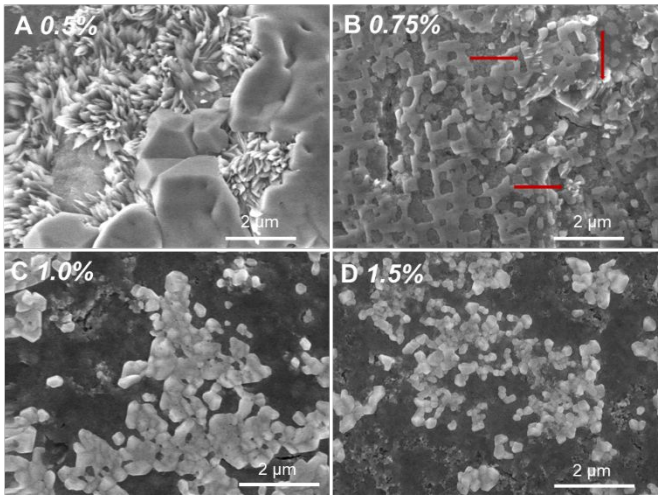

Fig. 2 Evolution of the morphology of TiO_2 precipitated by sfGFP-Car9 after 24h of reaction in gels with different agarose concentrations. Representative scanning electron micrographs show the appearance of the precipitates at the indicated agarose weight percentages.

To better understand the role of the hydrogel, we conducted mineralization experiments in the RDC using sfGFP-Car9 as an inducer and agarose concentrations ranging from 0.5% to 1.5%. After 24h of reaction, we observed a progression of morphologies as the agarose weight percentage increased: monolithic precipitates with unique peripheral features (Fig. 2A) gave way to heavily bridged (Fig. 2B) and more loosely connected particles (Fig. 2C) and eventually to rather well dispersed nanoparticles that were smaller in size (Fig. 2D). We

attribute these distinct morphological outcomes to the fine interplay of reaction and diffusion and explain our results as follows. In the absence of hydrogel (i.e., in the case of bulk precipitation), both TiBALDH precursor and protein inducer are uniformly abundant and titania growth is reaction limited. The displacement of lactate and citrate ligands by Car9 segments promotes polycondensation reactions between neighbouring Ti complexes in a process that may be facilitated by charge compensation between negatively charged titania clusters and positively charged regions of the sfGFP scaffold.[6, 8] Under such conditions, uncontrolled growth leads to extended branched precipitates lacking unique morphological features. At the highest agarose concentration employed here (1.5%), the process is inherently diffusion-limited and nearly spherical particles ranging in size from ~50 to 500 nm are produced (Fig. S11). This is because protein-stabilized clusters grow slowly due to a limited supply of TiBALDH.[17] Decreasing the agarose weight percentage to 1.0% also yields particles but their size increases (from ~200-nm to 1-µm; Fig. S6), likely because the flux of precursor also increases. A fine balance between TiBALDH diffusion and consumption at intermediate agarose concentrations (0.5-1.0%) leads to the production of precipitates that combine the characteristics of bulk-mineralized titania (e.g., large monoliths) with fine morphologies that have not, and in all likeliness cannot, be accessed through traditional bulk biomineralization schemes. For instance, the use of 0.75% agarose (Fig. 2B) yields a network of 543 ± 283 nm (n = 12) particles interconnected by narrower bridges (260 ± 114 nm; n = 12). This material also contains needles that are the hallmark of 0.5% agarose mineralization reactions (Fig. 2A). However, these needles are sparse and short (Fig. 2B, arrows; Fig. S12).

Previously, we used a series of rationally designed substitutions in the Car9 segment of sfGFP-Car9[9] to precipitate amorphous titania containing a small amount of nanocrystallites whose phase could be tuned from ~85% monoclinic to ~65% anatase depending on the identity of the mutation(s).[8] To determine if diffusional control would amplify these rather subtle effects, we first tested three of these mutants in the RDC using 1% agarose hydrogels and 24h of reaction. Loosely connected networks of spherical particles were observed in all cases (Fig. S13), with some variations in size distributions (Fig. S14) and a slight decrease in precipitate yield (Fig. S15), but no significant differences in morphology relative to the wild type protein (Fig. 2C). This is consistent with the progressive incorporation of all proteins within a slowly growing precipitate and isotropic growth under diffusion limited conditions.[18] In short, neither mutations affecting the charge (K8AK11A and R4QR12Q), or the structure (F6A) of the Car9 solid-binding peptide have a significant influence on morphological outcomes under conditions where the availability of the precursor is limited by diffusion.

On the other hand, the titania mineralized in the 0.5% hydrogel system exhibited two features: (1) large monolithic islands of precipitate; and (2), unique morphologies and crystallographic features that were typically located at the periphery of the large precipitates and depended on the identity of the protein inducer (Fig. 3 and S16). We attribute monolith formation to fast initial consumption of precursor in the reaction zone and to uncontrolled titania growth, much like what occurs under bulk precipitation conditions. As the reaction progresses, however, only a limited amount of precursor remains in the reaction zone, allowing for controlled titania growth into distinct

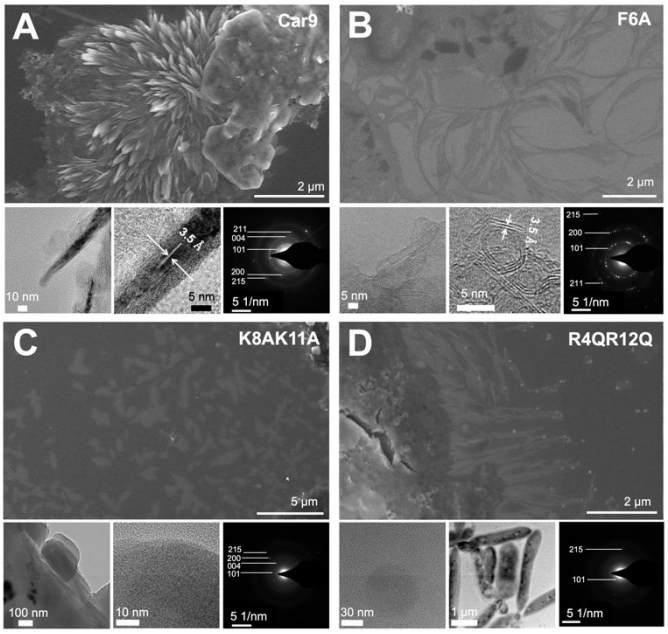

Fig. 3 SEM (top panels) and TEM (bottom panels) characterization of titania precipitates obtained using (A) wild type sfGFP-Car9, (B) sfGFP-Car9(F6A), (C) sfGFP-Car9(K8AK11A), and (D) sfGFP-Car9(R4QR12Q) as the protein inducer. All experiments were conducted in a RDC operated with a 0.5% agarose gel. Samples were excised after 24h of reaction. TEM imaging was conducted at low (bottom left) and high resolution (bottom center). Selected area diffraction (SAED) patterns (bottom right) were acquired on the high-resolution fields shown and are indexed to anatase titania. An enlarged version is provided as Fig. S16.

morphologies. Because x-ray diffraction and Raman spectroscopy were unsuitable for the analysis of our low yield samples and their unique mineral morphologies,[19] we employed SEM and TEM analysis to characterize both shape and crystallinity. Figure 3A and S16A shows that wild type sfGFP-Car9 induced the formation of dense bundles of needles with tapered ends at the edges of titania monoliths (also see Fig. 2A). These needles were ~656 ± 115-nm in length and 144 ± 42-nm in width (n =12) and had strong anatase signatures, as evidenced by indexing of selected area electron diffraction (SAED) patterns acquired in the TEM and a lattice spacing of 3.5Å in high-resolution TEM (HRTEM) images that is consistent with the 3.5Å separation distance of adjacent (101) planes in anatase TiO_2 (Fig. 3A and S16A). We note that the fabrication of morphologically similar needles and rods typically require harsh conditions and high temperature processing.[20-22] The F6A variant gave rise to thin and flexible thread-like structures that also exhibited strong anatase characteristics in SAED and HRTEM analysis (Fig. 3B and S16B). By contrast, the K8AK11A and R4QR12Q mutants induced the precipitation of plate- and peapod-like structures that were largely amorphous (Fig. 3C-D and S16C-D). A rhodamine degradation assay further revealed that the titania precipitated in-hydrogel by sfGFP-Car9 (and its R4QR12Q variant) had superior photocatalytic activity than the material obtained by bulk precipitation with the same protein (Fig. S17). We conclude that an RDC operated with a 0.5% agarose hydrogel allows access to a bioprecipitation regime that

greatly magnifies the morphogenetic effects of single or double amino acid substitutions in a solid-binding protein.

The F6A mutation was originally selected to increase the conformation flexibility of the Car9 peptide, a prediction borne out by molecular dynamics simulations[9] and calculations performed on the FlexPred server[23] (Fig. S18). The K8AK11A and R4QR12Q substitutions were chosen because they remove positively charged chains that have long been implicated in peptide binding to titania clusters.[24] However, the same mutations also reduce the ability of Car9 segments to self-associate at silica interfaces.[9] Collectively, these observations provide a possible explanation for the protein-specific TiO_2 morphologies observed in Fig. 3. Because they oligomerize under conditions of high surface occupancy,[9] sfGFP-Car9 and its F6A variant may have an enhanced ability to bring together pre-existing 2-5 nm anatase nanoparticles (Fig. S19) that are in equilibrium with liganded Ti(IV) species in TiBALDH solutions.[6, 8, 25, 26] They are also likely to be more effective at directing the growth of extended anatase features under the controlled operating environment of the RDC (Fig. 3). A more flexible F6A variant induces the formation of thread-like structures while the more rigid wild type Car9 peptide promotes the growth of long needles. The paucity of crystalline features in the titania mineralized by the K8AK11A and R4QR12Q mutants may be related to weaker interactions with negatively charged precursor species due to a lower number of positively charged side chains, and to a reduced propensity for oligomerization that diminishes the ability of these two proteins to direct the growth of crystalline facets even under controlled environments.[9]

To our knowledge, this is the first demonstration that single or double amino acid substitutions in a *ca*. 250 residues-long protein inducer can exert such a profound effect on the morphology and crystallography of a precipitated mineral. We anticipate that reaction-diffusion control will be valuable to study and design other biomineralizing proteins, and that it will prove broadly useful to access unique morphologies and crystallinities with a large range of biomolecule inducers and precursor species, obviating the need for harsh and energy-intensive processing conditions.

Author Contributions

K.P. conducted all experiments at the exception of TEM imaging and SAED acquisition. The sfGFP-Car9 fusion protein and its mutants were constructed and used by B.H. to lay out initial conditions for in-hydrogel titania mineralization. F.B. contributed to experimental design, data analysis, and managed the project. K.P. and F.B. wrote the manuscript.

Conflicts of interest

F.B. declares competing financial interest in Proteios Technology, Inc. which researches and commercializes Car9-based technologies.

Acknowledgments

We are grateful to Yatong Ge for help with RDC design and to Ellen Lavoie for TEM/SAED characterization. This material is based upon work supported by the U.S. Department of Energy, Office of Science, Office of Basic Energy Sciences, as part of the Energy Frontier Research Centers program: CSSAS, the Center for the Science of Synthesis Across Scales under Award Number DE-SC0019288. Part of this work was conducted at the Molecular Analysis Facility, a National Nanotechnology Coordinated Infrastructure site at the University of Washington which is supported in part by the National Science Foundation (grant NNCI-1542101), the University of Washington, the Molecular Engineering & Sciences Institute, and the Clean Energy Institute.

Notes and references

1. X. Chen and S. S. Mao, *Chem. Rev.*, 2007, **107**, 2891-2959.
2. J. Bai and B. Zhou, *Chem. Rev.*, 2014, **114**, 10131-10176.
3. Y. Lan, Y. Lu and Z. Ren, *Nano Energy*, 2013, **2**, 1031-1045.
4. J. L. Sumerel, W. Yang, D. Kisailus, J. C. Weaver, J. H. Choi and D. E. Morse, *Chem. Mater.*, 2003, **15**, 4804-4809.
5. A. Hernández-Gordillo, A. Hernández-Arana, A. Campero-Celis and L. I. Vera-Robles, *RSC Adv.*, 2019, **9**, 34559-34566.
6. G. A. Seisenbaeva, G. Daniel, J.-M. Nedelec and V. G. Kessler, *Nanoscale*, 2013, **5**, 3330-3336.
7. Z. Tong, Y. Jiang, D. Yang, J. Shi, S. Zhang, C. Liu and Z. Jiang, *RSC Adv.*, 2014, **4**, 12388-12403.
8. B. Hellner, A. E. Stegmann, K. Pushpavanam, M. J. Bailey and F. Baneyx, *Langmuir*, 2020, **36**, 8503-8510.
9. B. Hellner, S. Alamdari, H. Pyles, S. Zhang, A. Prakash, K. G. Sprenger, J. J. De Yoreo, D. Baker, J. Pfaendtner and F. Baneyx, *J. Am. Chem. Soc.*, 2020, **142**, 2355-2363.
10. E. Nakouzi and O. Steinbock, *Sci. Adv.*, 2016, **2**, e1601144.
11. A. Rao and H. Cölfen, *Biophys. Rev.*, 2016, **8**, 309-329.
12. D. Saliba, M. Ammar, M. Rammal, M. Al-Ghoul and M. Hmadeh, *J. Am. Chem. Soc.*, 2018, **140**, 1812-1823.
13. R. M. Walliser, F. Boudoire, E. Orosz, R. Tóth, A. Braun, E. C. Constable, Z. Rácz and I. Lagzi, *Langmuir*, 2015, **31**, 1828-1834.
14. H. Li and L. A. Estroff, *Adv. Mater.*, 2009, **21**, 470-473.
15. J.-D. Pédelacq, S. Cabantous, T. Tran, T. C. Terwilliger and G. S. Waldo, *Nat. Biotechnol.*, 2006, **24**, 79-88.
16. Y. Jiang, D. Yang, L. Zhang, L. Li, Q. Sun, Y. Zhang, J. Li and Z. Jiang, *Dalton Trans.*, 2008, 4165-4171.
17. T. Yang, J. Liu, J. Dai and Y. Han, *CrystEngComm*, 2017, **19**, 72-79.
18. N. T. K. Thanh, N. Maclean and S. Mahiddine, *Chem. Rev.*, 2014, **114**, 7610-7630.
19. M. El-Shetehy, A. Moradi, M. Maceroni, D. Reinhardt, A. Petri-Fink, B. Rothen-Rutishauser, F. Mauch and F. Schwab, *Nat. Nanotechnol.*, 2021, **16**, 344-353.
20. B.-M. Wen, C.-Y. Liu and Y. Liu, *New J. Chem.*, 2005, **29**, 969-971.
21. A. Sadeghzadeh Attar, M. Sasani Ghamsari, F. Hajiesmaeilbaigi, S. Mirdamadi, K. Katagiri and K. Koumoto, *J. Phys. D: Appl. Phys.*, 2008, **41**, 155318.
22. R.-C. Wang, C.-C. Hsu and S.-J. Chen, *Ind. Eng. Chem. Res.*, 2012, **51**, 3677-3681.
23. I. B. Kuznetsov and M. McDuffie, *Bioinformation*, 2008, **3**, 134-136.
24. S. Liu, X.-Y. Meng, J. M. Perez-Aguilar and R. Zhou, *Sci. Rep.*, 2016, **6**, 37761-37761.
25. H. Zhang and J. F. Banfield, *Chem. Mater.*, 2002, **14**, 4145-4154.
26. R. L. Penn and J. F. Banfield, *Geochim. Cosmochim. Acta*, 1999, **63**, 1549-1557.